



CHORUS

This is the accepted manuscript made available via CHORUS. The article has been published as:

# Nonlocal and Nonlinear Surface Plasmon Polaritons and Optical Spatial Solitons Induced by the Thermocapillary Effect

Shimon Rubin and Yeshaiahu Fainman

Phys. Rev. Lett. **120**, 243904 — Published 15 June 2018

DOI: [10.1103/PhysRevLett.120.243904](https://doi.org/10.1103/PhysRevLett.120.243904)

# Nonlocal and nonlinear surface plasmon polaritons and optical spatial solitons induced by the thermocapillary effect

Shimon Rubin<sup>1,\*</sup> and Yeshaiahu Fainman<sup>1</sup>

<sup>1</sup>*Department of Electrical and Computer Engineering, University of California, San Diego, 9500 Gilman Dr., La Jolla, California 92023, USA*

We study the propagation of surface plasmon polaritons (SPPs) on a metal surface which hosts a thin film of a liquid dielectric. The ohmic losses that are inherently present due to the coupling of SPPs to conductors' electron plasma, induce temperature gradients and fluid deformation driven by the thermocapillary effect, which lead to a nonlinear and nonlocal change of the effective dielectric constant. The latter extends beyond the regions of highest optical intensity and constitutes a novel thermally self-induced mechanism that affects the propagation of the SPPs. We derive the nonlinear and nonlocal Schrödinger equation (NNLSE) that describes propagation of low intensity SPP beams, and show analytically and numerically that it supports a novel optical spatial soliton excitation.

**Introduction:** Surface Plasmon Polaritons (SPPs) are electromagnetic excitations that propagate at the interface between a metal and a dielectric material [1, 2]. The unique properties of the SPPs that enable to concentrate light in a sub-wavelength region around the interface and SPPs' sensitivity to changes of the dielectric constant, have motivated numerous theoretical and experimental studies over the last few decades with a broad range of applications in bio-sensing [3], medicine [4], thermal/photo imaging [5, 6], and solar energy [7, 8]. The inherent Joule heat generation due to ohmic losses leads to an increase of the metal's temperature and affects the properties of nearby objects by heat conduction. While previous works investigated heating effects on fluids due to SPP heat generation, such as generation of Rayleigh-Bénard convection, [9, 10], thermophoretic migration of suspended particles [11, 12], gas-fluid phase transition [13], generation of micro-structures in polymer films [14] and transport of liquid droplets [15] - to the best of our knowledge the effect of the fluid on SPP due to self-induced heating hasn't been reported to date.

In this work we theoretically study the interaction between a propagating SPP along a planar metal surface and an adjacent thin film of a dielectric liquid. Fig.(1a) presents a schematic description of the problem; a spatially non-uniform SPP beam propagates along the  $z$  direction and locally heats the metal, which in turn heats the gas-fluid interface. Local increase of the free interface temperature leads to a surface tension gradient and triggers the thermocapillary effect [16] (a special case of the Marangoni effect [17]), manifested by thermocapillary flows with a distinctive shape of Bénard cells [18] and deformation of the free interface. A local temperature increase usually leads to a decrease of the surface tension in the hotter region, and to interfacial flows from the hotter region to the colder region, though few liquids are known to exhibit an opposite behavior of the surface tension [19], both

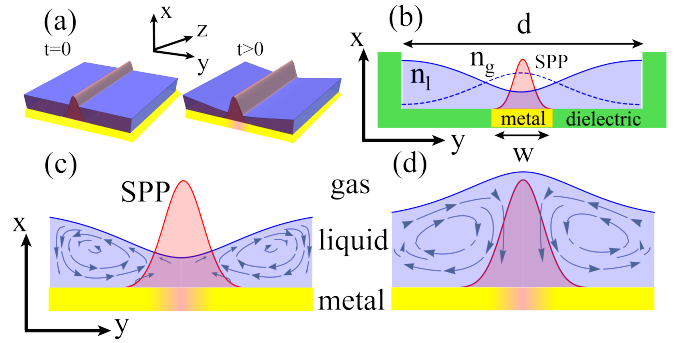


FIG. 1. (a) 3D scheme of a propagating SPP along the  $z$  axis on a metal surface near a thin liquid film; left - uniform thin film of thickness  $h_0$  prior to heating effects; right - deformed thin film after SPP generates nonuniform temperature field. (b) normal cross section of a propagating SPP along a metal of a finite width  $w$  embedded within a fluidic slot of width  $d$ , (c,d) normal sections presenting thermocapillary flows (blue arrows) and the deformed free interface for positive and negative Marangoni constant, respectively, for the case  $w$  and  $d$  are larger than the width of the SPP beam.

illustrated in Fig.(1c) and Fig.(1d). In case the liquid film is thinner than the penetration depth of the SPP into the bulk, the liquid deformation is coupled back to the Maxwell equations through the changes of the liquid's dielectric constant, and together with the heat transport form a complete set of coupled equations. This novel SPP-fluid coupling mechanism induces changes in the geometrical shape of the thin film of a liquid dielectric, which is fundamentally different from the traditional thermo-optical effect, where the source of dielectric function changes stems from changes of material density and polarization. Importantly, the resultant change of the liquid's refractive index is spatially nonlocal, in a sense that the induced fluid deformation extends beyond the regions of highest optical intensity to more distant regions. Prominent mechanisms that are known to admit a light-induced nonlocal index response are: charge transport in photorefractive crystals [20],

atomic diffusion in atomic vapors [21, 22], heat transport and changes of volume/atomic polarizability [23], molecular long-range interaction in nematic liquid crystals [24–26], coupling of lasing disordered resonators via directional stimulated emission [27] and quantum effects on the Thomas-Fermi screening length [28, 29]. Several of these nonlocal mechanisms support optical solitons, which are localized intensities of light intensity due to a balance between diffraction and nonlinearity of the medium, and have been in the focus of an active research for the last few decades (see [30, 31] and references within).

In this letter we derive NNLSE for an SPP under thermocapillary induced nonlocal nonlinearity in the dielectric material and then show that it supports a novel spatial soliton excitation - an SPP that propagates on a metal covered with a thin liquid film and a dynamical fluidic plasmonic photonic crystal (FPPC) with intensity tunable bandgap. We show that our model naturally admits a strongly nonlocal limit of the Snyder-Mitchell accessible soliton model [32], and present numerical results that describe diffraction of two SPP beams analogous to the Young double slit experiment.

**Governing equations for the non-linear media:** Our starting point is the Navier-Stokes equations for a non-compressible fluid of viscosity  $\mu$ , mass density  $\rho$ , velocity field  $u_i$  and stress tensor  $\tau_{ij}$  for Newtonian fluid given by [33]

$$\rho(\partial_t u_i + u_j \partial_j u_i) = \partial_j \tau_{ij}; \quad i, j = x, y, z, \quad (1)$$

The free surface of the thin film, which rests on a metal surface (Fig.(1a)), satisfies the following stress balance equation [33]

$$\tau_{ij} n_j = \sigma n_i \vec{\nabla} \cdot \hat{n} - \vec{\nabla}_{\parallel} \sigma, \quad (2)$$

where,  $\sigma$  is the surface tension,  $\vec{\nabla} \cdot \hat{n}$  is the divergence of the normal and  $\vec{\nabla}_{\parallel}$  stands for a gradient with respect to the in-plane coordinates ( $y, z$ ). In this work we assume that the surface tension depends on temperature via [34]

$$\sigma(T) = \sigma_0 - \sigma_T \Delta T; \quad \Delta T \equiv T - T_0, \quad (3)$$

where  $\sigma_T$  is the Marangoni constant known to exhibit nearly temperature independent values over a large range of temperature for many materials [35], and the temperature field in the metal,  $T^m$ , is governed by the following 2D equation

$$\frac{\partial T^m}{\partial t} - D_{th}^m \nabla_{\parallel}^2 T^m = \frac{\Delta T}{I_0 \tau_{th}} \chi I; \quad \chi \equiv \frac{\alpha_{th}^m d^2 I_0}{k_{th}^m \Delta T}, \quad (4)$$

where the superscript  $m$  stands for quantities in the metal and  $I$  is an optical intensity of typical strength  $I_0$ . Here,  $D_{th}^m = k_{th}^m / (\rho^m c_p^m)$  is the heat diffusion coefficient;

$\rho^m, c_p^m, k_{th}^m, \alpha_{th}^m$  are the mass density, specific heat, heat conductance, and optical absorption coefficient, respectively;  $\tau_{th} = d^2 / D_{th}^m$  is the typical time scale;  $d$  is the typical length scale along the in-plane direction;  $\chi$  is the dimensionless intensity of the heat source.

Applying low Reynolds number and thin film assumptions (i.e. lubrication approximation) [36, 37], allows to neglect the inertial terms in the Navier-Stokes equations, Eq.(1), and drop the in-plane derivatives relative to the normal derivative. Together with the thin film limit of the matching conditions, Eq.(2), [38] yields the following equation for the thin film deformation  $\eta$

$$\frac{\partial \eta}{\partial t} + D_{\sigma} \nabla_{\parallel}^4 \eta = -\frac{\sigma_T h_0^2}{2\mu} \nabla_{\parallel}^2 T^m; \quad D_{\sigma} \equiv \sigma_0 h_0^3 / (3\mu), \quad (5)$$

which includes the effects of surface tension and thermocapillarity. Effects of gravity are negligible on a microscale and expected to emerge on a much larger scales comparable to the capillary length, [40], whereas non-retarded van der Waals interaction can be neglected for films with thickness above 100 nm [41]. The forces on a dielectric film due to non-homogeneity of the dielectric function on the free surface and electrostriction [42], are expected to have much lower magnitude than the thermocapillary effect [39].

Taking advantage of the linearity of the thermal transport and the thin film equations and assuming quasi-static temperature field distribution, which for transient problems typically holds at  $t > \tau_{th}$ , we can represent the deformation  $\eta$  in terms of the Green's function  $G_l$  of Eq.(5) and intensity as [39]

$$\eta(\vec{r}_{\parallel}, t) / h_0 = -M \int d\vec{r}'_{\parallel} dt' \frac{1}{\tau_{th}} G_l(\vec{r}_{\parallel} - \vec{r}'_{\parallel}, t - t') I(\vec{r}'_{\parallel}, t') / I_0. \quad (6)$$

Here,  $M \equiv \text{Ma} \cdot \chi / 2$  and  $\text{Ma} = \sigma_T \Delta T h_0 / (\mu D_{th}^m)$  is the dimensionless Marangoni number which represents the ratio between the surface tension stresses due to the thermocapillary effect, and dissipative forces due to fluid viscosity and thermal diffusivity. The typical values of the time scales  $\tau_l, \tau_{th}$  and  $\tau_{el}$ , that govern the transport of liquid, heat and propagation of SPP, respectively, satisfy

$$\tau_{el} \ll \tau_{th} \ll \tau_l = d^4 / D_{\sigma}. \quad (7)$$

Indeed, for the following values  $d = 1 \mu\text{m}$ ,  $h_0 = 0.25 \mu\text{m}$ ,  $D_{th}^m = 10^{-4} \text{m}^2 \text{s}^{-1}$ ,  $D_{th} = 10^{-7} \text{m}^2 \text{s}^{-1}$ ,  $\mu = 10^{-3} \text{Pa}\cdot\text{s}$ ,  $\sigma_T = 10^{-4} \text{Nm}^{-1} \text{K}^{-1}$ ,  $\sigma_0 = 10^{-3} \text{Nm}^{-1}$  we learn that  $\tau_l = 10^{-4} \text{s}$ ,  $\tau_{th} = 10^{-8} \text{s}$ , are much larger than  $\tau_{el} = 1/\omega = 10^{-14} \text{s}$  and Eq.(7) holds. The additional time scale that governs heat diffusion from the metal to the free surface,  $h_0^2 / D_{th}$ , is on the order of magnitude  $10^{-6} \text{s}$ , which is still much smaller than  $\tau_l$ .

**Nonlocal and nonlinear SPP:** We now utilize perturbation theory accounting for the propagation and

diffraction of an SPP on a metal-dielectric interface, incorporating dissipation as well as nonlinear and nonlocal effects. We start our analysis from the time independent Maxwell equations for TM waves. Combining the sourceless Maxwell equations, yields the following equations for the electric field,  $E_i^{m,d}$  [1, 2],

$$\partial_{ij}^2 E_j^{(m,d)} - \partial_{jj}^2 E_i^{(m,d)} = k_0^2 \epsilon(\vec{r}) E_i^{(m,d)}; \quad k_0 = \omega/c, \quad (8)$$

where  $i$  labels the different equations ( $i = x, y, z$ ),  $j$  is a summation index which runs on all values  $j \neq i$ , and  $m, d$  stand for the metal and dielectric regions, respectively. Employing the depth averaged approximation [43], we treat the gas-fluid bilayer as a single media with an effective index calculated by averaging the index above the metal ( $x > 0$ ) weighted by the decay factor  $2q_d e^{-2q_d x}$ . Specifically, integrating the index distribution  $n_l$  (liquid) between  $0 < x < h_0 + \eta$  and  $n_g$  (gas) for  $x > h_0 + \eta$  yields the corresponding changes of the depth averaged index and the dielectric constant [39]

$$\begin{aligned} \Delta n_D(\eta) &= \tilde{b} \eta(\vec{r}_{\parallel}, t)/h_0; \quad \tilde{b} = 2q_d h_0 (n_l - n_g) e^{-2q_d h_0}; \\ \Delta \epsilon_D(\eta) &= b \eta(\vec{r}_{\parallel}, t)/h_0; \quad b = 2n_0 \tilde{b}, \end{aligned} \quad (9)$$

respectively. Here, we kept the leading term in the  $\eta/h_0$  series,  $q_d^2 = \beta_0^2 (1 - \epsilon_D)$ ,  $\beta_0 = k_0 \sqrt{\epsilon_m \epsilon_D / (\epsilon_m + \epsilon_D)}$ ,  $n_0 = \sqrt{\epsilon_D} = n_l - (n_l - n_g) e^{-2q_d h_0}$  and the dimensionless deformation,  $\eta/h_0$ , is determined by Eq.(6). Employing perturbative expansion in dimensionless number  $M$  of the governing equations for SPP in the metal, dielectric with depth averaged dielectric function,  $\Delta \epsilon_D$ , and the matching conditions between metal and dielectric, we derive the following NNLSSE [39]

$$2i\beta_0 \frac{\partial A}{\partial z} + \frac{\partial^2 A}{\partial y^2} + \tilde{\chi}_{TC} A \int d\vec{r}'_{\parallel} dt' G_l(\vec{r}_{\parallel} - \vec{r}'_{\parallel}, t - t') |A|^2 = 0, \quad (10)$$

where  $\tilde{\chi}_{TC} = k_0^2 \chi_{TC} / (I_0 \tau_h)$  and  $A(y, z)$  is the envelope of the SPP beam [39]. Here,  $\chi_{TC}$  is a dimensionless number, given by  $\chi_{TC} = f b M$  and incorporates the effects of thermocapillarity, kinematics of the index averaged model and plasmonic enhancement [44] through the dimensionless numbers  $M$ ,  $b$  and  $f$ , respectively (see [39] for expression for  $f$  and [45, 46] for an alternative derivation).

**The limit of local interaction:** Consider the case schematically presented in Fig.(1b), where SPP of vacuum wavelength  $\lambda$  is restricted to propagate along a metal slab of width,  $w$ , which is smaller than the width of the fluidic slot,  $d$ . Furthermore, we assume that  $w \gg \lambda$ , which allows to neglect edge and other effects due to strong lateral confinement which lead to an enriched mode spectrum [47]. Therefore, we can assume that SPP admits the form of a non-diffracting beam, and following [48] the corresponding matching

conditions at  $x = 0$  lead to the following dispersion relation

$$\beta_0 \epsilon_m E_z^{(m)} \Big|_{x=0} = i q_m (n_0^2 + \Delta \epsilon_D(\eta)) E_x^{(d)} \Big|_{x=0}. \quad (11)$$

Next, let us determine the temperature distribution and the resulting thin film deformation due to an SPP that begins to propagate along the slab at  $t = 0$ . To this end, we determine the Green's functions,  $G_{th}$  and  $G_l$  which satisfy, respectively, Eq.(4) and Eq.(5) with a source term  $\delta(x - x_0)H(t)$ , where  $H(t)$  is Heaviside function. For convenience, we consider the case where the thin film forms an angle  $\pi/2$  with the walls at  $x = 0, d$ , whereas the temperature field satisfies Dirichlet boundary conditions at the edges  $x = (d \pm w)/2$ . Employing the closure relation [49], we derive the corresponding expressions for  $G_l$  and  $G_{th}$  [39], which upon convolving with Gaussian intensity leads to the following closed form expression for  $\eta$  [39]

$$\frac{\eta(y, t)}{h_0} = -\frac{2dM\tau_l I}{3\pi^6 \tau_{th} I_0} \sum_{n=1}^{\infty} \frac{(-1)^n}{\lambda_n n^4} \varphi_n(y) \varphi_n\left(\frac{w}{2}\right) \left(1 - e^{-\lambda_n \frac{t}{\tau_l}}\right). \quad (12)$$

Here,  $\lambda_n$  is a constant (see [39]) and  $\varphi_n(y) = \sqrt{2/d} \cos(n\pi y/d)$  is the set of the eigenfunctions associated with the corresponding Sturm-Liouville problem.

Fig.(1b) presents the fluid deformation given by Eq.(12), showing that in the limit  $w \ll d$ , the length scale that governs  $\eta$  is set by the width of the slot  $d$ . Consequently, we can approximate the change of the dielectric constant Eq.(9) along the metal slab, by the value of the deformation at the center,  $\eta(d/2, t \rightarrow \infty)$ . In this limit the nonlinearity is reduced to a local Kerr-like cubic nonlinearity and the index change,  $\Delta n_D$  can be represented as either  $\Delta n_D = \alpha_{TC} \Delta T$  or  $\Delta n_D = n_2 |E_0|^2$ , resembling index changes invoked due to traditional thermo-optical and electro-optical effects, where [39]

$$n_2 = \frac{4}{\pi^6} \frac{\sigma_T}{\sigma_0} \frac{d^4}{h_0} \frac{\alpha_{th}^m}{k_{th}^m}, \quad \alpha_{TC} = \frac{3b}{2\pi^3} \frac{\sigma_T}{\sigma_0} \frac{d^4}{w^2 h_0^2}. \quad (13)$$

It is instructive to compare index changes invoked by the thermocapillary effect,  $\Delta n_{TC}$ , to changes triggered by traditional thermo-optical effect,  $\Delta n_{TO} = \alpha_{TO} \Delta T$  where  $\alpha_{TO}$  is the thermo-optical coefficient. Assuming the values given below Eq.(7), and  $\lambda = 800$  nm,  $\alpha_{TO} = 10^{-4} \text{ K}^{-1}$ ,  $w = 5 \mu\text{m}$ ,  $d = 15 \mu\text{m}$ , and utilizing Eq.(9), yields  $\alpha_{TC}/\alpha_{TO} \simeq 10^5$ . The latter indicates that similar index changes,  $\Delta n_{TO}$  and  $\Delta n_{TC}$ , require much smaller temperature increase for the case of the thermocapillary effect. In practice, this ratio is expected to be smaller due to thermal radiation losses and thermal advection.

Interestingly, thin film deformation driven by the thermocapillary effect introduces substantial changes of both real and imaginary parts of the dielectric

function depending on the dielectric properties of the liquid. Utilizing perturbation expansion of Eq.(11) in the local Kerr-like nonlinearity limit, we can express SPP momentum with leading correction as  $\beta = \beta_0 + \Delta\beta$ , where  $\Delta\beta = \Delta\epsilon_D \beta_0 q_d (q_d^2 + \beta_0^2) / (2\epsilon_D^2 (q_d' + q_d))$  [50],  $q_d^2 = \beta_0^2 (1 - \epsilon_D)$  and  $q_d' = \text{Re}(q_d)$ . The corresponding phase change  $\Delta\beta$  vanishes for  $\beta_0 = 0$  and tends to  $-\Delta\epsilon_D \omega_p / (2(1 + \epsilon_D)^{3/2})$  as  $\beta_0 \rightarrow \infty$ , where  $\omega_p$  is the plasma frequency in the metal. In particular, in case  $\text{Im}(\epsilon_D) > 0$ , changes of fluid thickness lead to power dependent changes of the real part of the depth averaged index as well as enhanced gain proportional to  $M$ . This is inherently different than other gain mechanisms such as the electronic nonlinearity resulting from one- or two-photon processes [51].

Consider now the case of self-induced change in dispersion relation due to four SPP beams that propagate on a metal slab of width,  $w$  which has a size similar to the fluidic slot,  $d$ , and satisfy  $\lambda \ll w, d$ . Furthermore, assume that these waves admit equal amplitude,  $|E_0|^2$ , propagate along the directions  $(\pm\hat{y} \pm \hat{z})/\sqrt{2}$  and admit a wavefront larger than the size of the fluidic cell. Treating these beams as a plane waves yields the following optically induced intensity distribution,  $16|E_0|^2 \cos^2(\beta_0 x/\sqrt{2}) \cos^2(\beta_0 y/\sqrt{2})$ , and upon inserting it into Eq.(6) yields the following deformation [39]

$$\frac{\eta(\vec{r}_{\parallel}, \infty)}{h_0} = -\frac{\tau_l}{16\tau_{th}\lambda_N} M \cdot \cos\left(\beta_0 x/\sqrt{2}\right) \cos\left(\beta_0 y/\sqrt{2}\right), \quad (14)$$

shown in Fig.(2a), where  $N$  is an integer given by  $N = \beta_0 d / (\sqrt{2}\pi)$  and  $\lambda_n$  is a constant given in [39]. The deformation described by Eq.(14) admits a discrete translation symmetry along the  $y, z$  axes, and constitutes an FPPC for a lower power SPP that propagates in this background over distances lower than its decay length. Specifically, Fig.(2b) presents the projection of the photonic band structure on the surface Brillouin zone for two different cases with different thicknesses  $h_0 = 150$  nm and  $h_0 = 200$  nm and periodicity 500 nm, obtained by utilizing a commercial-grade simulator based on the finite-difference time-domain method [52]. To maximize the effect of the liquid, we have chosen the liquid index of value  $n_l = 2$ , which is slightly below the index of selenium monobromide with  $n_l = 2.1$ . [53]

**Nonlocal effects:** Consider a single SPP beam of a finite spatial width,  $\sigma_{SPP}$ , that begins to propagate at  $t = 0$  along an infinite metal surface covered with a thin liquid film. The response of the thin film can be determined by the corresponding Green's function,  $G_l$ , of Eq.(5) with a source term  $\delta(y)f(t)$ . Film dynamics can be probed by considering an exponentially relaxing source with  $f(t) = e^{-t/t_s}$ , where  $t_s$  is the relaxation time scale. The corresponding Green's function that vanishes

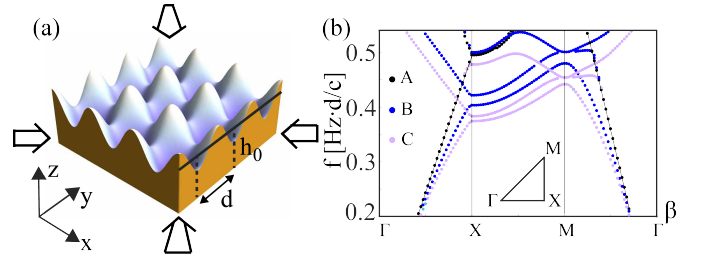


FIG. 2. (a) Surface deformation given by Eq.(14), optically induced by four SPPs (directions are indicated by arrows). (b) Bandstructure diagrams of the emerging FPPC for the cases: (B)  $h_0 = 200$  nm and (C)  $h_0 = 150$  nm. (A) presents the case without a liquid. Complete bandgap occurs for  $n = 3$  (not shown), which is beyond the reach of current technology.

in the limit of large times is given by [39]

$$G_l(y) = -\frac{1}{D_\sigma} e^{-|y|/l_s} (\cos(|y|/l_s) + \sin(|y|/l_s)), \quad (15)$$

where  $l_s$  is the corresponding length scale given by  $l_s = (4D_\sigma t_s)^{1/4}$  that can be tuned by choosing sufficiently large decay time scale  $t_s$ . Importantly, the Green's function Eq.(15) admits Taylor expansion at the origin and therefore allows to implement the Snyder-Mitchell model [32], applicable for the strongly nonlocal regime. Expanding the Green's function inside the integral, Eq.(10), as  $G_l^{(0)} + \frac{1}{2}(y-y')^2 \partial^2 G_l^{(0)} / \partial y^2$  yields a local Schrödinger equation with a harmonic oscillator potential

$$2i\beta_0 \frac{\partial \psi}{\partial z} = -\frac{\partial^2 \psi}{\partial y^2} - \tilde{\chi}_{TC} I^{(0)} \frac{\partial^2 G_l^{(0)}}{\partial y^2} y^2 \psi, \quad (16)$$

where  $\psi = e^{-iz\tilde{\chi}_{TC} I^{(0)} \beta_0^* / (2|\beta_0|^2)} A$ ,  $\partial^2 G_l^{(0)} / \partial y^2 = 2/(D_\sigma l_s^2)$ ,  $I^{(0)}$  is the integral of  $|A|^2$  along the  $yz$  plane and  $\beta_0^*$  is the complex conjugate of  $\beta_0$ . Notably, the sign of the potential term is determined by the sign of the Marangoni constant, and  $\tilde{\chi}_{TC} < 0$  simultaneously guarantees a Gaussian soliton [39], analogous to the solution obtained in [32], and an exponentially damping factor,  $e^{z\tilde{\chi}_{TC} I^{(0)} \text{Im}(\beta_0) / (2|\beta_0|^2)}$ , along the propagation direction which captures dissipation effects.

To demonstrate the effect of nonlocality in case the correlation length due to the thermocapillary effect is comparable to  $\sigma_{SPP}$ , we turn to commercial numerical solver [54] and implement built-in Explicit Runge Kutta method. Fig.(3) presents an interference pattern of two parallel SPP Gaussian beams of spatial variance  $\sigma_{SPP}$ , analogous to Young's double-slit experiment in a leading order of a small parameter  $\tilde{\chi}_{TC}$ . In this approximation, the effect of the nonlocal self-induced spatial index change is taken into account by evaluating the integral in Eq.(10) along the input beam (see Fig.(3d,e,f)) [39]. Fig.(3a,b,c) present diffraction patterns

of two SPPs due to negative, zero and positive Marangoni constant, respectively, that lead to induced dielectric function (empty graph) and temperature (dashed line). Notably, the index gradients required to support the self-focusing and defocusing effects in (a) and (c), respectively, are determined by the gradients of the optical beams intensities whereas the temperature field gradient is set by the much larger size of the metal slab. The self-focusing effect presented in Fig.(3a) yields solitary wave solutions where the deformed liquid acts as a waveguide for SPP beams.

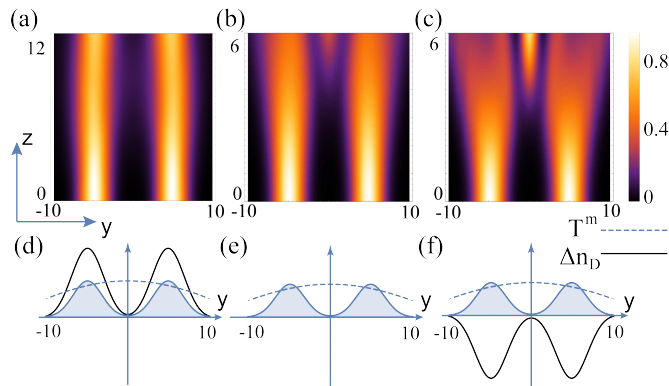


FIG. 3. Numerical results presenting diffraction pattern of two SPPs for: (a)  $\sigma_T < 0$ , (b)  $\sigma_T = 0$  and (c)  $\sigma_T > 0$ . (d,e,f) present thin film shape (solid line), the optical intensity at  $z = 0$  (filled line) and the corresponding temperature distribution (dashed line) [39]. Relevant parameters:  $\sigma_{SPP} = 2.5/\sqrt{2}$ ,  $\eta/h_0=0.2$ ,  $\lambda = 800$  nm  $h_0 = 200$  nm,  $n_l = 2$ ,  $n_g = 1$ ; coordinate axes normalized with respect to  $k_0$ .

**Summary and concluding remarks:** We presented a theoretical and numerical analysis of a novel thermocapillary self-induced, nonlocal and nonlinear mechanism for SPP-fluid interaction. In contrast to the traditional thermo-optical effect where the dielectric function modulation stems from changes of material density and polarization, the thermocapillary effect induces changes of the geometrical shape of the thin film. This generates waveguide-like structures in the fluid film, and exhibits much longer response time and correlation length than other nonlocal mechanisms reported to date. The coupling described in this work is readily applicable to other optical systems with heat dissipation such as photonic waveguides [55] and more general fluidic systems such as fluid-fluid interfaces, and may be applicable for thermal imaging. Furthermore, dynamic modulation of other basic properties of the optical lattice such as symmetry and periodicity, opens a door to utilize our plasmonic system as a quantum simulator of a many body quantum systems such as topological insulators [56] recently realized in photonic systems [57, 58].

**Acknowledgments:** S.R. cordially thanks Brandon Hong, Dr. Shiva Shahin and Dr. Valeri Frumkin for

fruitful discussions. This work was supported by the Office of Naval Research (ONR), Multidisciplinary University Research Initiative (MURI), the National Science Foundation (NSF) (Grants DMR-1707641, CBET-1704085, ECCS-1405234, ECCS-1644647, CCF-1640227 and ECCS-1507146), the NSF ERC CIAN, the Semiconductor Research Corporation (SRC), the Defense Advanced Research Projects Agency (DARPA), NSF's NNCI San Diego Nanotechnology Infrastructure (SDNI), the Army Research Office (ARO), and the Cymer Corporation.

\* rubin.shim@gmail.com

- [1] H. Raether, *Surface plasmons on smooth and rough surfaces and on gratings*. Springer-Verlag Berlin, (2013).
- [2] S. A. Maier, *Plasmonics: fundamentals and applications*. Springer Science & Business Media, (2007).
- [3] J. N. Anker, et al., *Nat. Mater.* **7.6**, 442, (2008).
- [4] A. M. Gobin, et al., *Nano Lett.* **7.7**, 1929, (2007).
- [5] M. Mecklenburg, et al. *Science* **347.6222**, 629, (2015).
- [6] I. Goykhman, B. Desiatov, J. B. Khurgin and U. Levy, *Nano. Lett.* **11**, 2219 (2011).
- [7] H. A. Atwater and A. Polman, *Nat. Mater.* **9.3**, 205, (2010).
- [8] S. Linic, P. Christopher, and D. B. Ingram. *Nat. Mater.* **10.12**, 911, (2011).
- [9] B. J. Roxworthy, A.M. Bhuiya, S. S. P. Vanka and K. C. Toussaint Jr., *Nat. Commun.* **1**, (2014).
- [10] J. S. Donner, G. Baffou, D. McCloskey and R. Quidant, *ACS nano* **5.7**, 5457 (2011).
- [11] J. C. Ndukaife, et al., *Nat. Nanotechnol.* **11.1**, 53 (2016).
- [12] L. Lin, et al. *ACS nano* **11.3**, 3147 (2017).
- [13] A. O. Govorov and H. H. Richardson, *Nano Today* **2.1**, 30 (2007).
- [14] L. Röntzsch, et al., *Appl. Phys. Lett.* **90.4**, 044105 (2007).
- [15] A. Passian, et al., *Phys. Rev. E* **73.6**, 066311 (2006).
- [16] J. R. A. Pearson, *J. Fluid Mech.* **4.5**, 489 (1958).
- [17] C. G. M. Marangoni, *Ann. Phys. Chem.* **219**, 337 (1871).
- [18] H. Bénard, *Rev. Gen. Sci. Pures Appl.* **11**, 1261 (1900).
- [19] K. K. Cheng and C. Park, *Heat Mass Transf.*, **1** (2017).
- [20] G. C. Duree Jr, et al., *Phys. Rev. Lett.* **71.4**, 533 (1993).
- [21] D. Suter and T. Blasberg, *Phys. Rev. A* **48.6**, 4583 (1993).
- [22] S. Skupin, M. Saffman and W. Krolikowski, *Phys. Rev. Lett.* **98.26**, 263902 (2007).
- [23] C. Rotschild, et al., *Phys. Rev. Lett.* **95.21**, 213904 (2005).
- [24] D. W. McLaughlin, et al., *Physica D* **88.1**, 55 (1995).
- [25] C. Conti, M. Peccianti and G. Assanto, *Phys. Rev. Lett.* **91.7**, 073901 (2003).
- [26] G. Assanto and M. Peccianti, *IEEE J. Quantum Electron.*, **39.1**, 13 (2003).
- [27] M. Leonetti, C. Conti, and C. Lopez., *Light: Science & Applications* **2.8**, e88 (2013).
- [28] D.C. Marinica, et al., *Nano Lett.* **12.3**, 1333 (2012).
- [29] J. Zuloaga, E. Prodan and P. Nordlander, *Nano Lett.* **9.2**, 887 (2009).
- [30] Z. Chen, M. Segev, and D. N. Christodoulides, *Rep. Prog. Phys.* **75**, 086401 (2012).
- [31] Y. S. Kivshar and G. Agrawal. *Optical solitons: from fibers to photonic crystals.*, Academic press, (2003).
- [32] A. W. Snyder and D. J. Mitchell, *Science* **276.5318**, 1538

- (1997).
- [33] L. D. Landau and E. M. Lifshitz, *Fluid mechanics*, Course of Theoretical Physics vol.6., Elsevier, (1987).
- [34] V. G. Levich, *Physicochemical hydrodynamics*. Prentice hall, (1962).
- [35] A. W. Adamson, *Physical Chemistry of Surfaces*, 5th ed., Wiley, New York, (1990).
- [36] J. Happel and H. Brenner, *Low Reynolds number hydrodynamics: with special applications to particulate media. Vol. 1*. Springer Science & Business Media, (2012).
- [37] S. Howison, *Practical applied mathematics: modelling, analysis, approximation.*, No. 38. Cambridge university press, (2005), ch. 20.
- [38] A. Oron, S. H. Davis, and S. G. Bankoff, Rev. Mod. Phys. **69.3**, 931 (1997), Eq.(2.17) and Eq.(2.28).
- [39] See Supplemental Material at [url] for additional details, which includes Refs. [59-61].
- [40] P.-G. de Gennes, F. Brochard-Wyart and D. Quéré. *Capillarity and wetting phenomena: drops, bubbles, pearls, waves*. Springer Science & Business Media, (2013).
- [41] J. N. Israelachvili, *Intermolecular and surface forces*, Academic Press, Burlington (2011).
- [42] L. D. Landau, L. P. Pitaevskii and E. M. Lifshitz, *Electrodynamics of continuous media*. Vol. 8. Elsevier, (2013).
- [43] L. S. Jung, C. T. Campbell, T. M. Chinowsky, M. N. Mar, and S. S. Yee, Langmuir, **14.19**, 5636 (1998).
- [44] A. Marini and D. V. Skryabin, Phys. Rev. A **81.3**, 033850 (2010).
- [45] E. Feigenbaum and M. Orenstein, Opt. Lett. **32**, 674 (2007).
- [46] A. R. Davoyan, I. V. Shadrivov, and Y. S. Kivshar, Opt. Express **17.24**, 21732 (2009).
- [47] P. Berini, Adv. Opt. Photonics **1.3**, 458 (2009).
- [48] D. Mihalache et al., Opt. Lett. **12.3**, 187 (1987).
- [49] G. B. Arfken and H. J. Weber. *Mathematical methods for physicists*, Elsevier Inc. (1999).
- [50] A. Marini, et al., Optics letters **34.18**, 2864 (2009).
- [51] R. W. Boyd, *Nonlinear optics*, Academic Press, (2003).
- [52] FDTD Solutions Lumerical Inc. version. 8.18.1332, <http://www.lumerical.com/tcad-products/fdtd/>.
- [53] R. Meyrowitz, Am. Mineral **40**, 398 (1955).
- [54] Wolfram Research, Inc., Mathematica, Version 11, Champaign, IL (2017).
- [55] K. Padmaraju and K. Bergman, Nanophotonics, **3**, 269 (2014).
- [56] F. D. M. Haldane, Phys. Rev. Lett. **61**, 2015 (1988).
- [57] M. C. Rechtsman, et al., Nature **496.7444**, 196 (2013).
- [58] M. Hafezi, S. Mittal, J. Fan, A. Migdall, and J. M. Taylor, Nature Photonics **7.12**, 1001 (2013).
- [59] J. A. Stratton, *Electromagnetic theory*, IEEE Press, (2007).
- [60] J. S. Jakobs and A. W. Lawson, J. Chem. Phys. **20**, 1161 (1952).
- [61] J. W. Cahn, J. Chem. Phys. **42.1**, 93 (1965).